Engineered Science

REVIEW PAPER

View Article Online

An Overview of Electrically Conductive Polymer Nanocomposites toward Electromagnetic Interference Shielding

Longfei Lyu,[1] Jiurong Liu,*[1] Hu Liu,[2] Chuntai Liu,*[2] Yang Lu,[3] Kai Sun,[4,5] Runhua Fan,[4] Ning Wang,[6] Na Lu,[7] Zhanhu Guo*[5] and Evan K. Wujcik*[3]

A comprehensive overview of the up-to-date research activities targeting electromagnetic interference (EMI) shielding is provided, focusing on the multifunctional polymer nanocomposites (PNCs) reinforced with a variety of conductive fillers. The unique dielectric, magnetic and other physicochemical properties derived from certain morphology-, composition-, and loading-controlled nanostructures for EMI shielding behaviors are elaborated. The conductive fillers including three different categories: carbon, metals, and conductive polymers in the EMI shielding PNCs are discussed together with their synergistic effects on enhancing the EMI shielding property. The enhanced electromagnetic interference shielding effectiveness and mechanisms are discussed with detailed examples and are envisioned to provide rational design of next generation lightweight EMI shielding materials.

Keywords: Polymer Nanocomposites; Conductive Fillers; EMI shielding

Received 18th April 2018, Accepted 17th May 2018

DOI: 10.30919/es8d615

1. Introduction

Electromagnetic interference (EMI) shielding is an effective method of using a material which can effectively lower the transmittance of electromagnetic wave to reflect or absorb the electromagnetic radiation. Because electromagnetic radiation regularly occurs at high frequencies and strongly interferes with electronics, electromagnetic interference (EMI) shielding is of particular importance to electronics.[1,2] Reflection is one of the most commonly observed EMI shielding mechanisms.[3–6] In order to acquire good electromagnetic interference shielding effect, free-moving electrons or holes are the prerequisites for the shielding material. The magnitude of loss from reflection is proportional to the electrical conductivity (σ) of the shielding material. Therefore, electrically conductive materials are preferred EM shielding absorbers, even though a high σ is not necessary. For example, the volume resistivity of carbon nanotubes (CNTs) is less than 1 Ω·cm, yet it is sufficient to demonstrate the EMI effect.[7] The σ value will not be taken as a scientific pre requisite for EMI shielding due to the fact that the conducting connectivity is not a requirement.[1] Although not required, the shielding can be enhanced by a large σ. For conductive materials including metals and carbon, the existence of their conducting connectivity is exhibited by their high σ. Metals are widely used as EMI shielding materials. Their reflection function under EM radiation is caused by the existence of free electrons.[1] Another important mechanism is absorption.[8–10] The material must own dipoles for strong EM wave absorption.[1] The electric dipoles present shielding materials with a high dielectric constant (ε), while the magnetic dipoles give shielding materials a high μ value.[11,12] The absorption loss and reflection loss are a function that depends on the σ_r, the electrical conductivity, and μ_r, the relative magnetic permeability. Because of their high σ, metals like silver and copper could reflect more electromagnetic waves. Similarly, super-permalloy (a magnetic alloy, with about 20% iron and 80% nickel) has a high μ so this material shows excellent absorption. Compared to the μ_r value of a few thousand for ordinary steel, commercial permalloy and MuMetal® typically have relative permeability around 100,000 and 80,000-100,000, respectively. As the EM wave frequency

[1] *Key Laboratory for Liquid–Solid Structural Evolution and Processing of Materials, Ministry of Education and School of Materials Science and Engineering, Shandong University, Jinan, Shandong 250061, China. E-mail: jrliu@sdu.edu.cn*
[2] *National Engineering Research Center for Advanced Polymer Processing Technology, Zhengzhou University, Zhengzhou, 450002, China. E-mail: ctliu@zzu.edu.cn*
[3] *Materials Engineering and Nanosensor [MEAN] Laboratory, Department of Chemical and Biological Engineering, The University of Alabama, Tuscaloosa, AL, USA. E-mail: Evan.Wujcik@ua.edu*
[4] *College of Ocean Science and Engineering, Shanghai Maritime University, Shanghai 201306, China*
[5] *Integrated Composites Laboratory (ICL), Department of Chemical & Biomolecular Engineering, University of Tennessee, Knoxville, TN 37996, USA. E-mail: zguo10@utk.edu*
[6] *State Key Laboratory of Marine Resource Utilization in South China Sea, Hainan University, Haikou, P. R. China*
[7] *Lyles School of Civil Engineering, School of Materials Engineering, Purdue University, West Lafayette, IN, USA*

increases, the loss from reflection decreases whereas the loss from absorption increases.[1] Besides, multiple reflections are also critical for shielding mechanism, which EM wave reflects at muti-interfaces in a shielding material.[13] The requirement for multiple reflections is a large specific surface area in contact with the EM waves. A highly porous or foam material can provide a large specific surface area, while a composite material consisting of fillers with large surface areas and matrix can also provide large interfacial areas. Both large surface and interfacial areas can result in multiple reflections, which further enhance the EMI shielding performance. Electrically conductive polymer nanocomposites use polymer as the matrix while incorporating different kinds of conductive fillers to make the inherently electrical insulating polymer conductive. The polymer matrix has merits including low cost, excellent chemical and oxidation resistance, great processability and low density. The conductive filler gives properties such as large surface and interfacial area, electrical conductivity, and magnetic permeability into the nanocomposite making it promising in EMI shielding. The commonly used conductive fillers include carbon materials, metal nanostructures, intrinsic conductive polymers and various combination of aforementioned fillers.

The EM shielding is commonly expressed in decibels. The shielding effectiveness (SE, in dB) involves all of these losses. The intrinsic properties of shielding materials restrict the shielding effectiveness in the broad frequency range (i.e. 200 MHz to 18 GHz). This includes the σ , ε, EM source frequency, and the vertical dimension between the EM source and the material.[14] Meanwhile, the absorption loss has a close relationship with the thickness (d) of the material. In order to achieve highly effective EM shielding, an EMI shielding material needs to be able to (1) reach high shielding capability with 99% absorption of the incoming EM waves (20 dB) required for human safety[15] and (2) active EMI shielding within a wide frequency range. For example, in spite of the advantages of metals for EMI shielding, their large density, instable chemical property, and narrow absorbed frequency are considered major drawbacks for effective EMI shielding.[16] In contrast, polymers have many advantages including low density, ease of processability, and low cost, yet many can be penetrated by EM waves through their insulating interfaces. Therefore, polymer nanocomposites (PNCs) with electrically conductive fillers well distributed within the electrically insulating polymer matrices are one of the best strategies to overcome the metal-related problems for EMI shielding.

Three types of conductive PNCs are typically utilized to achieve EMI shielding, the first being polymer/conductive carbon filler system. For example, the reflection loss (RL) obtained by using 7 wt% carbon nanotubes (CNTs) in a polystyrene matrix was found to be 18.2-19.3 dB in X-band.[17] However, simply by using materials with increased conductivity, a high reflection loss is difficult to realize.[18,19] Another type of commonly used conductive PNCs for EMI shielding is polymer/metal-loaded ferromagnetic nanoparticles (NPs). These are advantageous due to the fact that, theoretically, magnetic nanostructures such as iron NPs can provide high absorption on account of their high magnetization.[20,21] However, the permeability is drastically affected by the ferromagnetic resonance and is decreased in GHz range.[22,23] Besides, both low magneto-crystalline anisotropy and permeability limit the SE of these ferromagnetic metal-loaded PNCs.[24] The third common conductive system is conductive polymers and their composites. For example, polyaniline (PANI) PNCs have been shown as effective microwave absorbents due to their unique electrical properties, controllable dielectric loss, simple synthesis, stable performance, anti-corrosion, and cost efficiency.[25–29] Other conductive polymer-based PNCs have also demonstrated excellent EMI shielding capabilities including polypyrrole (PPy)[30] and polyphenyl amine[31] based PNCs. The σ of conducting polymers can be manipulated through different doping agents to absorb more electromagnetic waves for high-need applications (for instance RL $>$ 40 dB for commercial usage).[28] Multilayer films or coatings using conducting polymers are becoming candidates for the shielding filter.[14] One option is to deposit conducting polymers on flexible fabrics for EMI shielding.[32] Meanwhile, the embedment of NPs such as carbon nanofillers into the conducting polymers is of great interest due to the interactions between conducting polymer structure and the surfaces of the nanofillers at the particle-polymer interface.[33]

Designing a shielding material with a particular level of attenuation and specific physical criteria will not be easy. The design combines shielding mechanism with factors such as a complex relationship among the intrinsic electromagnetic properties of shielding materials and reasonable extrinsic parameters (such as absorber thickness and frequency range). Understanding important design parameters and relevant measurement techniques, we propose the method of preparing shielding materials. In Fig. 1, the reflections can cause damages in the case of EM radiation emitted by electronic circuits because of interferences among transistor T, resistor R and chips. Hence, the interferences can be damaged or malfunctioned by the reflected EM waves. In order to resolve these detrimental effects by reaching $P_r \approx 0$ meanwhile keeping $P_o \approx 0$, one material should be designed to satisfy the attenuation of the EM waves and mitigated through the conductive dissipation.[16]

The ε and μ are typically out of balance for polymer/carbon nanofiller PNCs, leading to a consequence that most of EM waves are reflected instead of being absorbed. This is considered a major drawback for their use in EMI shielding. In other words, conductive materials such as carbon and metal tend to reflect EM waves. Hence, a good match between ε and μ in a shielding material can result in effective absorption, while a multi-layer shield barrier with larger surface area and interfacial area would favor multi-reflections. In this overview, we focus on the EMI shielding performance and mechanism of PNCs reinforced with different conductive fillers. The unique morphology-, composition-, and loading-controlled EMI shielding performances of different systems are critically reviewed. In addition, other EMI shielding PNCs based on the combination of different conductive fillers are also covered. Finally, the prospective of conductive EMI shielding materials is provided.

2. Criteria to evaluate the shielding effectiveness

When encountered with an incident EM wave, the mathematical expression of the SE is

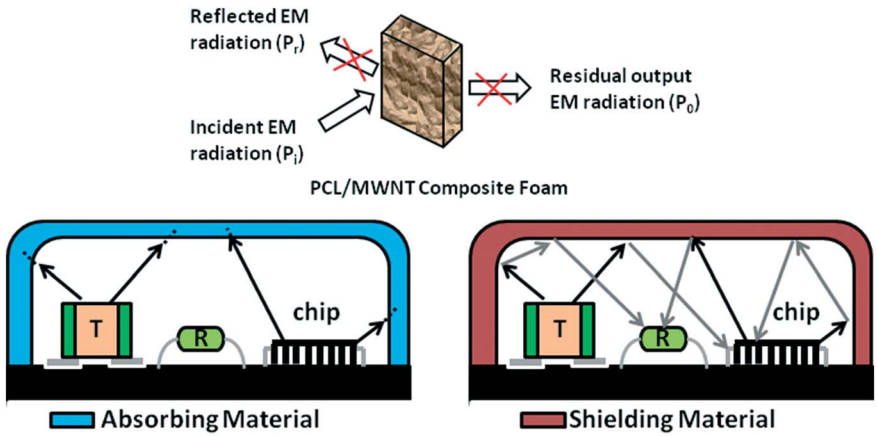

Fig. 1 The differences between an EMI shielding and absorbing coating in an electronic device.[16]Adapted with permissions from Royal Society of Chemistry.

$$\mathrm{SE} = 10\ log\left(\frac{P_i}{P_o}\right) \tag{1}$$

where P_i is the incident electromagnetic wave intensity on the surface of a material and P_o is the penetrable electromagnetic wave intensity through a material, respectively. In view of the theoretical principle, the evaluation of SE will be discussed according to the intrinsic properties of the shielding materials as well as the loss tangent (tan δ). Meanwhile, three types of shielding materials will be classified via emphasizing one of these three parameters (σ, ε and μ) in each material.

2.1. Conductive shielding materials with negligible magnetic property

Eq. (2) describes all the components of the total shielding efficiency:[14,34,35]

$$SE_T = 10\ log\ (P_i / P_o) = SE_A + SE_R + SE_I \tag{2}$$

$$SE_A = 20k_2 dloge = 8.68k_2 d \tag{3}$$

$$SE_R = 20\ log\frac{|1+n|^2}{4|n|} \tag{4}$$

$$SE_I = 20\ log\left|1-\frac{(1-n)^2}{(1+n)^2}exp\left(2ikd\right)\right| \tag{5}$$

where d is the distance which the EM waves travelled through the shielding material and the parameters k_2 (is the absorption coefficient, also named as α), n (is one of the influential factors of the complex wave vector k $(k = n\frac{\omega}{c} = n\frac{2\pi}{\lambda_0})$, and k are defined by the following equations.

$$k_2 = \left(\frac{2\pi}{\lambda_0}\right)\sqrt{\frac{\varepsilon_r'\left(\sqrt{1+tan^2\delta}\mp 1\right)}{2}} \tag{6}$$

$$n = \sqrt{\frac{\varepsilon_r'(\sqrt{1+tan^2\delta}\pm 1)}{2}} + i\sqrt{\frac{\varepsilon_r'(\sqrt{1+tan^2\delta}\mp 1)}{2}} \tag{7}$$

$$k = \left(\frac{2\pi}{\lambda_0}\right)\sqrt{\frac{\varepsilon_r'\left(\sqrt{1+tan^2\delta}\pm 1\right)}{2}} + i\left(\frac{2\pi}{\lambda_0}\right)\sqrt{\frac{\varepsilon_r'\left(\sqrt{1+tan^2\delta}\mp 1\right)}{2}} \tag{8}$$

where SE_A is the absorption shielding efficiency, SE_R is reflection shielding efficiency. and SE_I is multiple reflection efficiency. When $SE_A \geq 15$ dB, the SE_I must be considered in order to measure exactly.[35–37] The explicit description of terms in Equation (2) is[14,35]

where λ_0 is the wave length, ε_r' represents the real part of complex relative permittivity ($\varepsilon_r = \varepsilon_r' + i\varepsilon_r''$), and the ± and ∓ signs are applied for positive and negative ε_r', respectively. The term tan δ, $\tan\delta = \varepsilon_r''/\varepsilon_r'$, characterizes the capability of transformating the electromagnetic energy to heat energy, where ε_r" is the imaginary part of ε_r, and ω is the angular frequency of the EM waves ($\omega = 2\pi f$), where f is the frequency, ε_0 is the dielectric constant in free space, and σ is the conductivity. Thus, large values of tan δ and ε_r" (usually named as loss factor) would indicate a better absorbing material.[36]

For an EMI shielding material consisting of multilayer films (Fig. 2), the multiple RL needs to be considered in addition to the loss from absorption and reflection.[14]

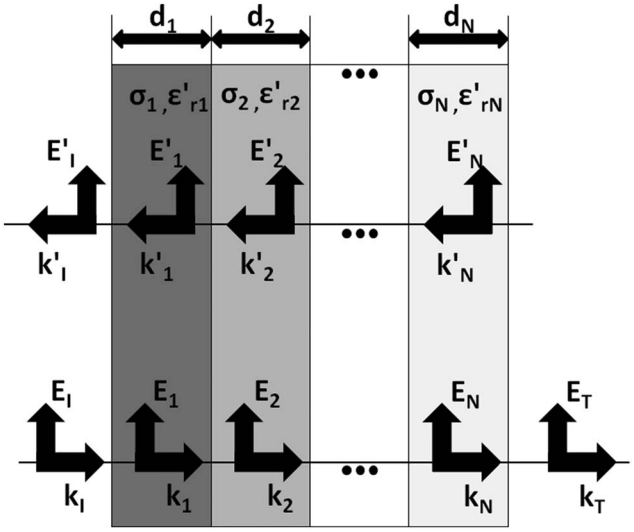

Fig. 2 For multilayer films, the direction of wave vectors, electric and magnetic field.[14]Adapted with permissions from American Institute of Physics.

For instance, in the j^{th} layer, the incident EM waves are in the form of E_j and E_j' means the reflected EM waves. The σ_j, ε_{rj} and d_j represent the electrical conductivity, the dielectric constant, and the thickness of the j^{th} layer, respectively. Assumed that the relative magnetic permeability, μ_r is 1. From an analysis of the boundary conditions, the internal regularities between the electric fields of EM waves in relation to multilayer structures could be revealed:[14]

$$\begin{bmatrix} E_I \\ E_I^{'} \end{bmatrix} = \begin{bmatrix} 1 & 1 \\ k_I & -k_I \end{bmatrix} A_1 B_1^{-1} A_2 B_2^{-1} \cdots A_N B_N^{-1} \begin{bmatrix} 1 \\ k_T \end{bmatrix} E_T \quad (9)$$

Here, matrices A_j and B_j are described as

$$A_j = \begin{bmatrix} 1 & 1 \\ k_j & -k_j \end{bmatrix} \quad (10)$$

$$B_j = \begin{bmatrix} exp(ik_j d_j) & exp(-ik_j d_j) \\ k_j exp(ik_j d_j) & -k_j exp(-ik_j d_j) \end{bmatrix} \quad (11)$$

where k_I correspond to the wave vectors in the incident medium and k_T correspond to the wave vectors in the transmitted medium, respectively. The k_j, the complex wave vector in the j^{th} layer is represented by Eq.12:[14]

$$k_j^2 = \omega^2 \mu_0 \varepsilon_0 \varepsilon_{rj}' + i\omega\mu_0\sigma_j \quad (12)$$

where μ_0 is the magnetic permeability of air, based on this , the real part k_{j1} and imaginary part k_{j2} (sometimes denoted as α, the absorption coefficient, and here Eq. (14) is the same as Eq. (6)); of complex wave vector k_j are given by:[14]

$$k_{j1} = \left(\frac{\omega}{c}\right)\sqrt{(|\varepsilon_{rj}'|/2)\left(\sqrt{1+tan^2\delta_j} \pm 1\right)} \quad (13)$$

$$k_{j2} = \left(\frac{\omega}{c}\right)\sqrt{(|\varepsilon_{rj}'|/2)\left(\sqrt{1+tan^2\delta_j} \mp 1\right)} \quad (14)$$

where, ε_{rj}' represents the real part of permittivity, and the ± and ∓ signs are applied for positive and negative ε_{rj}, respectively; c is the speed of EM waves in free space; and $tan\delta_j = \sigma_j / (\omega\varepsilon_0\varepsilon_{rj}')$ is the loss tangent (or dissipation factor) of the j^{th} layer.

Meanwhile, Eq. (8) describes the k (k_1+ik_2) in the monolayer film and means the complex wave vector. Again, through the relation $\lambda_0 = \frac{2\pi c}{\omega}$ (where λ_0 is the wave length), we can further get $\frac{\omega}{c} = \frac{2\pi}{\lambda_0}$, therefore, Eq. (8) becomes

$$k = k_1 + ik_2 = \left(\frac{\omega}{c}\right)\sqrt{(|\varepsilon_r'|/2)\left(\sqrt{1+tan^2\delta} \pm 1\right)} + i\left(\frac{\omega}{c}\right)\sqrt{(|\varepsilon_r'|/2)\left(\sqrt{1+tan^2\delta} \mp 1\right)} \quad (15)$$

Under the condition that the sign of ε_r' is in a special frequency range (i.e., tan $\delta >> 1$), $k_1 = k_2$ makes sense, while in a high-frequency range, when $k_2 = 0$, the ε_r' is positive. When $k_1 = 0$, the ε_r' is negative (i.e., tan$\delta << 1$).[14] From Eq. (9), the reflectance $R = \left|E_I^{'} / E_I\right|^2$ and the transmittance $T = \left|E_T / E_I\right|^2$ can be calculated directly.[14] Meanwhile, the absorbance A is obtained by using the relations (A+R+T= 1). The total shielding efficiency of the multilayer ($SE_{multi(T)}$) can be discribed as:[14]

$$SE_{multi(T)} = -10 \log T \quad (16)$$

The calculation of shielding response of monolayer film is much the same as the calculation of SE_{multi}. The total SE of monolayer film ($SE_{mono(T)}$) is described as:[14]

$$SE_{mono(T)} = 20\log\left|(1/4n)[(1+n)^2 \exp(-ikd) - (1-n)^2 \exp(ikd)]\right| \quad (17)$$

For positive ε_r', the $SE_{mono(T)}$ expresses two behaviors at different frequency, at low frequency the $SE_{mono(T)}$ has a constant behavior and an oscillating behavior occurs at high frequency which described by[14]

$$SE_{mono(T)} = 10\,P_1 + P_2 \cos(2\omega\sqrt{\varepsilon_r'}d/c) \quad (18)$$

Where P_1 and P_2 hold constants. We can deduce that $SE_{mono(T)}$ have the obvious characteristics oscillation period by $T_\omega = \pi c / \sqrt{\varepsilon_r} d$ at high frequency.

For negative ε_r', the $SE_{mono(T)}$ also has a constant behavior at low frequency, and it will only increases, based on the equation

$$SE_{mono(T)} = 10N_1 + N_2 \exp(2\omega\sqrt{\varepsilon_r'}d/c) \quad (19)$$

N_1 and N_2 are constants at high frequency.[14]

When the shielding efficiency satisfies two hypotheses, one is the source is far from the shielding barrier, and another is they both are not conform to near-shielding effects, the estimation that the SE is in the far-field limit,[34] through the change of k_2 (or α), n, and d , that ε_r' and σ_{ac} are the two parameter of the value of SE_T, will also change it;. By these equations, the requirement for high SE is higher ε_r' and σ_{ac}. Besides ε_r' and σ_{ac}, from varying the thickness of the material, SE_A and SE_I also can be successfully controlled.

The material with tan $\delta >> 1$ (ε_r" >> ε_r') is considered as a good conductor, otherwise, as a weak conductor. On the premise that tan$\delta >> 1$, the absorption coefficient α can be taken as $\alpha = (\omega\mu\sigma/2)^{1/2}$. This indicates that compared with ε_r, σ contributes a greater amount to the enhancement of the EMI shielding. On the premise that tan$\delta << 1$ and μ is the determining factor, the EM energy dissipation can also occur. However, when tan $\delta \approx 1$, σ_{ac} is just as important as ε_r' when predicting the shielding efficiency of a material.[7]

For an electrical conductor, EM radiations cannot penetrate all the region of the material, when it passes from air to material, they only pass the surface layer at high frequencies, and this is called the skin effect.[1] The distance at which the electric field intensity decreases to e^{-1} (e is the Euler's number, and e^{-1} is about 0.37) of the initial value is known as skin depth (Δ), which is definited by

$$\Delta = 1/\left(\pi f \mu \sigma\right)^{\frac{1}{2}} \quad (20)$$

where $\mu = \mu_0 \bullet \mu_r$, $\mu_0 = 4\pi \times 10^{-7}$ H m^{-1}.[1] The multiple-reflections represent the reflections at various interfaces in the shielding material. The big difference among absorption, reflection, and multiple-reflection is that the electromagnetic interference shielding efficiency can be decreased by only the multiple-reflection which must be considered in the condition of the thickness of shield materials above the threshold, Δ.[38]

Also note that depending on the skin effect, the size of filler in composite materials is a key factor of shielding effective. A filler size of 1 micron or less is typically preferred, thus CNTs and carbon nanofibers (CNFs) are promising fillers for preparing EMI shielding PNCs.

2.2. Conductive shielding materials with magnetic property

For the magnetic metallic materials with dielectric loss and magnetic loss properties (ε and μ), it is possible to formulate the RL as Eq. (21):[39]

$$RL = 20 \log \frac{\left|Z_{in} - Z_0\right|}{\left|Z_{in} + Z_0\right|} \quad (21)$$

where Z_0 is the impedance of free space; and Z_{in} is the input characteristic impedance, Eq. (22):

$$Z_{in} = Z_0 \sqrt{\frac{\mu_r}{\varepsilon_r}} \tanh\left\{ j(2\pi f d/c)\sqrt{\mu_r \varepsilon_r} \right\} \quad (22)$$

While magnetic NPs are limited by their intrinsic properties, the electromagnetic wave absorption behaviors of the metal magnetic nanomaterials have their inherent advantage of higher saturation magnetization (M_s). However, their high σ decreases the effective μ in high frequency drastically due to the skin effect - the tendency of an alternating electric current (σ_{AC}) to distribute itself within a conductor. With minimize the size of the monodispersed metallic particles below the skin depth, which can be easily achieved by embedding metallic magnetic NPs into non-conductive polymer matrices.

The high initial permeability (μ_i) of an EM wave absorbing material is necessary. For EM wave absorption applications and the μ_i of the material can be described as:[40,41]

$$\mu_i = \frac{M_s^2}{(ak_cH_cM_s + b\lambda\xi)} \quad (23)$$

where a and b depended by the intrinsic properties of materials, k_c is a proportion coefficient H_c is the coercivity, λ is the magnetostriction constant, and ξ is an elastic strain parameter of the crystal.[40] Meanwhile, K decide the direction of easy axis, which can be expressed as:[40]

$$K = k_cH_cM_s \quad (24)$$

Higher M_s and lower H_c are also good for the increase of μ_i so as to enhance the EM wave absorption. On the other hand, ε_r' and μ_r' represent the storage ability of EM energy, while ε_r" and μ_r" symbolize the loss ability.

In general, two prerequisites must be satisfied for an ideal EM wave absorption material, which are: (1) the impedance (Z) should be matching between air and the material, that is the ε_r and μ_r approximately equal in numerical value;[42,43] and (2) special physical structure gives the material strong magnetic or/and dielectric loss properties.[43]

2.3. Theoretical analysis

2.3.1. Magnetic loss. Interacting with EM waves, magnetic materials usually have three types of energy losses: eddy current loss, magnetic hysteresis loss, and residual loss. One of the typical equations can express the magnetic loss of magnetic materials.

$$\frac{2\pi \tan\delta_m}{\mu} = ef + aB + c \tag{25}$$

where e, a, c, μ, $\tan\delta_m$, f and B represent the eddy current loss coefficient, magnetic hysteresis coefficient, residual loss, permeability of the absorber, magnetic loss tangent, frequency of EM wave and magnetic flux density, respectively.[43]

2.3.2. Eddy current loss. When a conducting material is placed in an alternating magnetic field, an induced current would be produced inside which would dissipate the energy eddy current loss, which represented by the eddy current loss coefficient (denoted as "e_c").[44] The "e_c" can therefore be expressed as:[45]

$$e_c = \frac{4\pi^2 \mu_0 d^2 \sigma}{3} \tag{26}$$

Which d is the thickness and σ is the electric conductivity. According to Eq. (26), large d and σ can increase the e_c for one material, however, high σ would limit its EMI shielding application. and the e_c was also affected by other factors such as orientation, surface states, and structure of material.[43,46]

2.3.3. Magnetic hysteresis loss. When the polarity of the magnetic field changes the molecules of the magnetic material is rearranged. The energy loss induced by rearrangement is called magnetic hysteresis loss. The two primary cause of the energy loss are irreversible domain movement and magnetic moment rotation; and magnetic hysteresis coefficient (denoted as a_m) at low magnetic flux density can be expressed as:[43]

$$a_m = \frac{8b}{3\mu_0 \mu^3} \tag{27}$$

where b, μ_0 and μ represent the Rayleigh constant, vacuum permeability, and permeability of the material.

2.3.4. Residual loss. With the exception of three losses mentioned before, nearly all the remaining loss can be attributed to residual loss[47] caused by the magnetic after-effect loss at low frequency and size resonance (tendency of a system to oscillate), ferromagnetic resonance, natural resonance and/or domain wall resonance at high frequency. The residual loss is dominant.

The above mechanisms suggest that via designing a shielding material with specific physical characteristics (such as an appropriate σ, high Ms and low e_c) and chemical construction the considerable magnetic loss will be given.[42,43,48]

3. Why EMI shielding polymer nanocomposites?

From a scientific point of view, nanocomposites have many unique structure and morphology merits which can be used to prepare EM wave absorpting materials in the GHz range. Meanwhile, low density, large absorption bandwidth, simple preparation methods, and low cost are also paramount to developing effective EM wave absorbing materials.[49] On the nano-scale, materials usually exhibit unique electric,[50–52] magnetic,[53–58] and optical properties,[59] owing to their small size, large surface area , and quantum tunnel effect.[60–64] More importantly, these excellent properties usually cannot be achieved by using the corresponding bulk materials. For example, large interfacial dielectric loss can be achieved by the interface polarization since large specific surface area of one nano-material can provide a great number of active atoms on its surface.[65–67]

For the EM wave absorbers using conductive materials including CNTs,[68–77] CNFs,[78] graphene,[79–81] and conductive polymers such as PANI[82–84] or PPy,[85–88] the utilization of PNCs is an effective way to obtain light-weight products as the density of the PNCs can be reduced significantly. For magnetic PNCs as EM wave absorbers,[89] although the high density of magnetic materials such as iron,[39] cobalt,[90] and nickel[91,92] would compromise the density of magnetic PNCs as light-weight EM wave absorbers, the limited percentage of magnetic components incorporated in the polymer matrix can still provide relatively light-weight magnetic EM wave absorbers compared to traditional metal-based systems. More importantly, synergistic effects among the nano-size components in one PNCs system can further enhance the absorption efficiency as well as introduce other advantages to the system.[93,94]

Different physical and chemical property of the electric and magnetic components can affect the EMI shielding performance of the resulted composites.[41,43] Magnetic and electrically conductive PNCs with unique nanostructures have been extensively studied, and proved to have great potentials to be applied as EMI shielding materials[95] and molecular electronics.[96] As electrically conductive polymer nanocomposites, though there is no definitive conclusion on the effect of filling loading due to complexity as it depends on materials morphology, structure, composition, filler-matrix interactions, types of nanofillers, size of nanofillers, etc. However, there is a general trend for most polymer nanocomposites for EMI shielding applications. The conductivity and EMI SE usually increases with the increase of filling loading of nanofillers as the magnetic and electric properties are derived from nanofillers. However, excessive nanofillers typically will aggregate together due to high surface energy, compromise the mechanical integrity, processability of nanocomposites, increase the density and cost. A comparison table of some recent reported electrically conductive polymer nanocomposites with their composition, frequency range, and EMI SE was given in Table 1.

3.1. Carbon based nanofillers

Carbon-based materials, such as carbon black,[105] porous graphitic carbon,[106] expanded and foliated graphite,[107,108] CNFs,[109–111] fullerenes,[112] and CNTs[16,69,75,77,113–118] have been substantially investigated for preparing PNCs, benefitting from their low density, high

Table 1 Comparison table of some recent reported electrically conductive polymer nanocomposites with their composition, frequency range, and EMI SE.

Composition	Frequency Range	Shielding Effectiveness	Ref
Polycaprolactone (PAL)/CNT	25~40 GHz	60~80 dB	16
Polystyrene (PS)/CNT	8~12 GHz	25~30 dB	97
Polyamide-6 (PA-6)/CNT	8.2~12.4 GHz	25 dB	98
Polycarbonate (PC)/ Acrylonitrile butadiene styrene(ABS)/ Nickel coated carbon fiber	1 GHz	47 dB	99
Polyaniline (PANI)/CNT	12.4~18 GHz	27.5~39.2 dB	100
Polyester (PET)/ Polypyrrole (PPy)	0.5~1.5 GHz	36 dB	101
Epoxy/Graphene	8.2~12.4 GHz	21 dB	102
Polyvinylidene fluoride(PVDF) /Graphene	8~12 GHz	18 dB	103
Cellulose/CNT	8~12 GHz	18.7~22.5 dB	104

corrosion resistance, as well as flexibility and processability.[119] For instance, CNTs are considered the best carbon filler if good dispersion can be reached in a polymer matrix. In addition, their supreme physicochemical properties can be attributed to their mechanical property, thermal stability, extremely high σ.[120,121] However, the tubular configuration of the CNTs leads to large surface area and high surface energy that can aggravate the agglomeration of them. It is imperative to achieve good dispersion for improved overall performance. Graphene, the proclaimed "wonder material",[122–127] has also been extensively studied for EMI shielding applications.[80,81,97,103,128]

For these carbon-based nanofillers in polymer matrices, because of these nanaofillers are nonmagnetic, the ε and μ are typically out of balance.[129] Hence, the material tend to reflect the EM wave rather than to absorb it. This is driven by impedance mismatch. Currently, it is still one of the major hurdles for their usage as suitable EMI shielding materials.[16] By augmenting the content of air in polymer matrices using open-cell foam, the impedance matching can be obtained. Though different types of carbon nanofillers have their own advantages and disadvantages. However, a study conducted by Al-Saleh has shown that at the same nanofiller loading, the nanocomposite performance of EMI SE, permittivity and electrical conductivity follows in the order of CNT > CNF > CB. The reason is CNT possesses the highest conductivity, aspect ratio and lowest loading electrical percolation threshold. The polymer matrix selected was acrylonitrile-butadiene-styrene.[8]

Jerome et al[16] reported PCL foams filled with MWNTs for EMI shielding through using two methods, melt blending and co-precipitation. As seen in Fig. 3, SE was observed to be up to 80 dB with an average of -8.5 dB reflectivity (R) at 0.25 vol% of MWCNTs. Based on the SEM images (Fig. 4) and the reflectivity, it can be known that the open-cell structure contributes to enhance the absorption performance.

The foaming of MWNT/PCL PNCs enables them to maintain the dielectric constant at a relative low range, i.e., below 4. It is obvious that the ε_r of the PCL foam is ~50% lower than that of unfoamed PCL PNCs (ε_r = 2.2). Therefore, the ε_r of foamed PCL PNCs containing 0.24 vol% MWCNTs is close to that of solid PCL PNCs whose ε_r is about 3.5 even though the σ is ~ 3 to 4 times higher. Not only so, the shielding performance of the sample of 0.107 vol% MWNT (foam) is about as same as the sample of 0.16 vol% MWNT (solid). Due to a lower R, the ε_r of the foamed sample is lower. Foaming can effectively enhance the specific area of PCL/MWNTs PNCs. So it is a simple and direct way to enforce SE in the 20-80 dB range and low R within 8-15 dB. These parameters are better than those reported,[78,130] for which the enhancement of EMI shielding efficiency only contributes to reflection. Indeed, the 15 wt% loading is enough to achieve high ε_r (>30) and result in a reflection phenomenon at the inner surface. The performance is attributed to not only absorption but also reflection as the main influence factor to the EMI shielding.

Lightweight porous graphene-based composites (Fig. 5) synthesized from embedding functionalized graphene sheets (FGS) into polystyrene (PS) matrix at a relatively low density have been demonstrated with effective EMI shielding.[97]

It is obvious that the contribution of EM wave reflection is negligible over the whole frequency range. Compared with GPS027, GPS045 exhibits excellent electromagnetic interference shielding properties. The average SE_{Total}, SE_A, and SE_R are 29, 27.7, and 1.3 dB (Fig. 6a,b). The results indicate that because of the porous structure, nearly all of the EM energy is dissipated as heat while little electromagnetic wave is reflected from the composite surface. This confirms that the sequence of the importance of the shielding efficiency is absorption and reflection in 8.2-12.4 GHz. The specific SE (SE per g/cm^3) of the sample GPS045 was the highest value of 64.4 dB·cm^3/g, which was superior to ever reported polymer based EMI shielding materials. This porous microstructure in the composites (Fig. 6c,d) is promising for using as a lightweight shielding material against EM radiation.

Zhang et al[80] reported an effective EM wave absorber made from chemically reduced graphene (CR-G) dispersed in poly-ethylene oxide (PEO) matrix("CR-G/PEO" composites). The CR-G/PEO composites exhibit high permittivity (Fig. 7) and very low RL value (Fig. 8), which have the potential as protection against EM radiation.

The authors claim that the key factor of excellent EM wave absorption property of the CR-G/PEO composites is the electrical conduction loss, dielectric relaxation, interface scattering, and multiple reflections (shown in Fig. 9), for which the electromagnetic energy can be transferred to heat energy. When incident EM waves arrive at the materials, the oscillatory current and boundary charges can induce dielectric relaxation and polarization because of the directional motion of charge carriers.[80] A pronounced interfacial scattering can also be formed due to the complex permittivity difference. Influenced by different complex permittivity between CR-G and PEO, a significant interfacial scattering behavior happens. The exfoliated CR-G sheets with high aspect ratio could disperse well in the PEO matrix so as to constitute conduction networks, ultimately leading to high conduction losses. The junction between CR-G sheets and the PEO matrix forms interfacial multi-poles which induce the dielectric relaxation and polarization. The influence factor of dielectric relaxation and polarization is the same as the

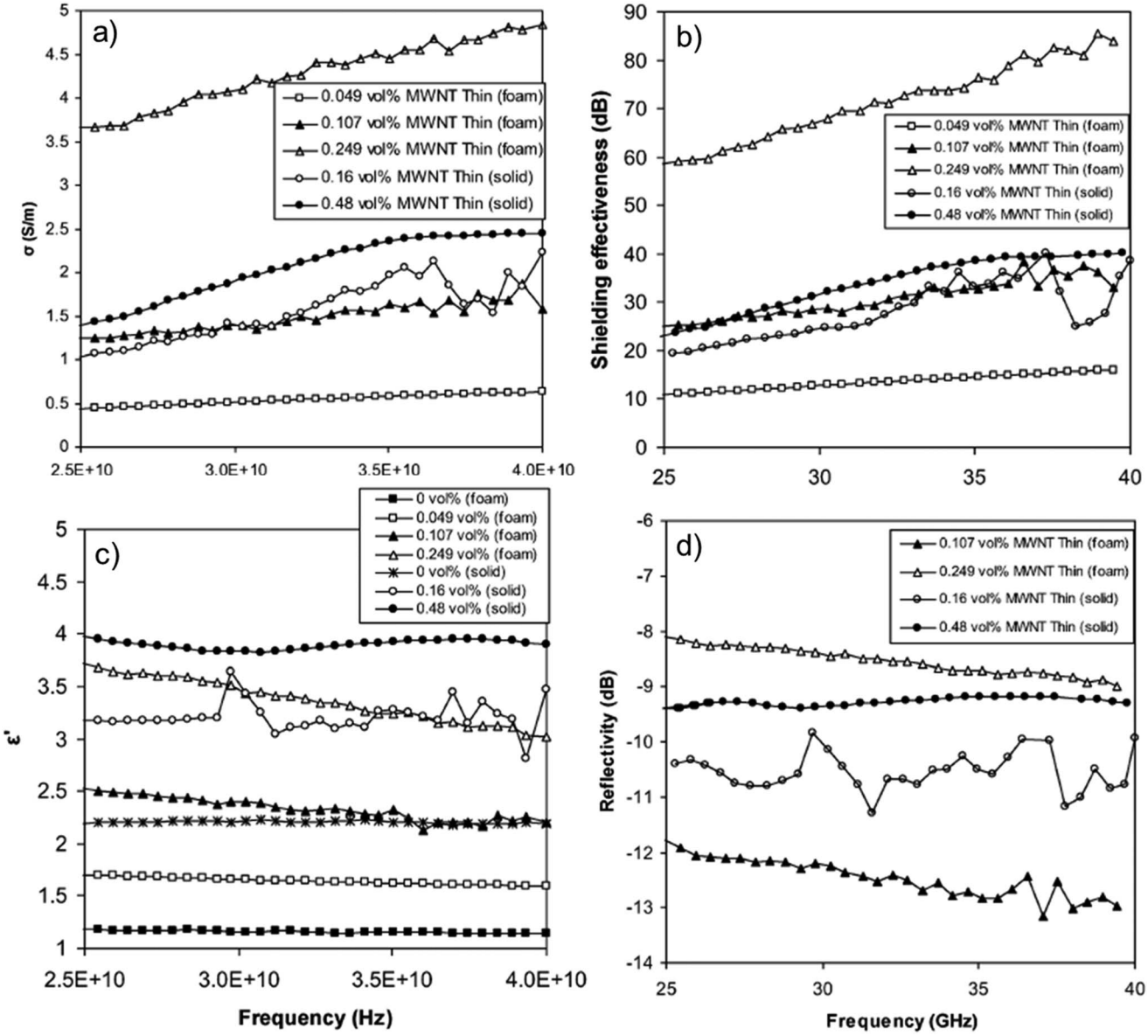

Fig. 3 Different EM properties of two types of multi-walled CNTs/polycaprolactone(PCL) PNCs: (a) σ, (b) SE, (c) ε_r, and (d) R.[16]Adapted with permissions from Royal Society of Chemistry.

interfacial scattering. In short, the high surface area could enhance the attenuation. Furthermore, ultrathin sheets and layered structure of CR-G contributes to strong multiple reflections (Fig. 9); thus, the way in which the electromagnetic wave propagates is the key factor to enhance the efficient absorption.

Recently, Hamed Azizi et al systematically research the impact construction of carbon-based nanofillers on EMI SE.[131] By adjusting the reaction temperature, the authors claim that compared with other shape cells, near-spherical cells in polymers own the highest reflection. The existence of air in the cell decreases the number of entering electromagnetic waves and the absorption property. So the open cell has better EMI SE than the close cell. The size of the cells is also an important factor that has impact on the performance. The smaller size of the cells acted as barriers to prevent the access of the electromagnetic waves and increasing the reflection.

The electromagnetic properties of carbon-based composite materials are excellent because carbon nanofillers and polymers are complementary. Among several factors, the filler-to-polymer ratio is important. Milana Trifkovic et al[98] adjust the mass of CNTs in two types of polymer matrices (polystyrene and polyamine-6, PA6) and evaluate their EMI SE. The authors claim that above CNT loadings of 0.3 wt%, the EMI SE of PS-CNT is higher than that of PA6-CNT. This phenomenon indicates that the percolation threshold of PS-CNT is 0.3 wt%, forming a conductive network and enhancing the EMI SE.

3.2. Metal based nanofillers

Magnetic NPs are ideal to be used as EMI shielding at high frequency over GHz because of their quantum size effect,[132,133] large specific surface area,[134] high surface atom percentage,[135] high Snoek's

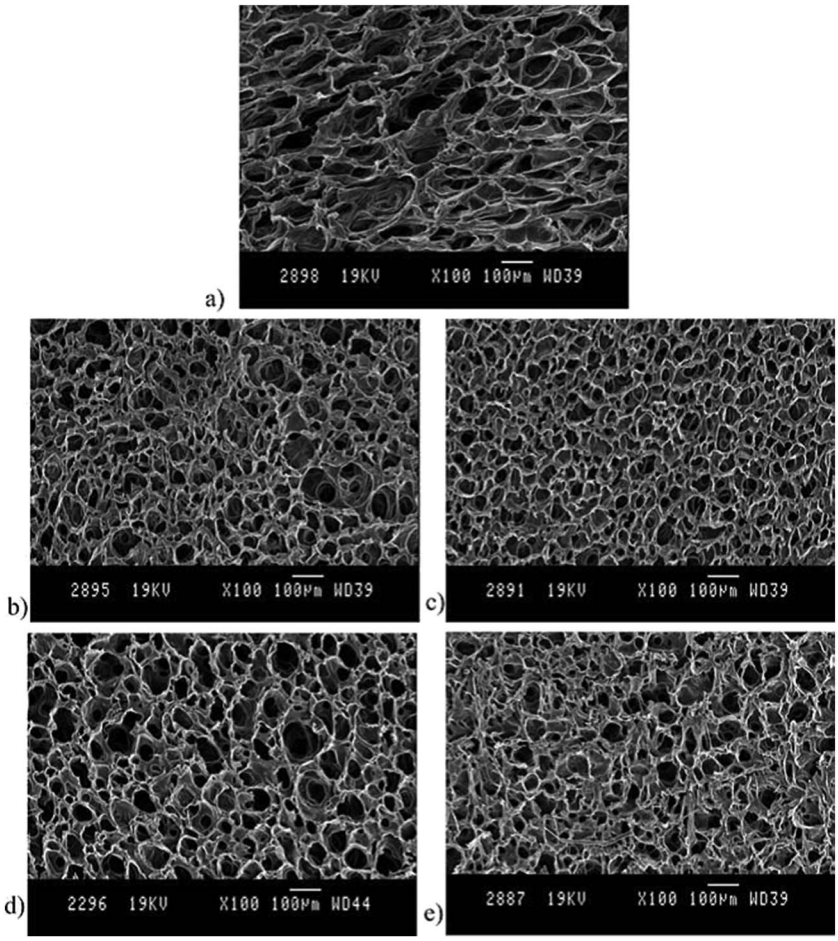

Fig. 4 SEM images of PCL foams filled with thin MWNTs: a) 0, b) 0.1 and c) 0.222 (melt-blending), d) 0.107 and e) 0.249 vol% (co-precipitation).[16]Adapted with permissions from Royal Society of Chemistry.

limit (a general bound for the family of initial permeability curves for various compositions of ferrites possessing cubic anisotropy).[136,137] Owing to these characteristic, magnetic NPs have strong interface polarization.[138] However, when incident EM waves reach the metallic magnetic material, the decrease of the relative complex permeability ($\mu_r = \mu' + i\mu''$) is inevitable because of the eddy current phenomenon.[139–141] The metallic magnetic nanomaterials such as Fe and Co,[32,142–144] are suitable candidates as EM wave absorbing materials with high magnetization values. Also, nickel[41,141,145,146] is another widely used EM wave absorbing material, which can attenuate EM waves mainly by the magnetic loss.[147,148]

For example, Han et al[41] reported the morphology-controlled synthesis of different nickel nanoparticles including five different morphologies and hexagonal Ni/Ni$(OH)_2$ nanoplates (illustrated in Fig. 10).

Compared with smooth chains and ring structure counterparts, based on the good matching between magnetic loss and dielectric loss, the enhanced EM wave absorption properties of Ni/Ni$(OH)_2$ plates is observed. Fig. 11 depicts ε'' in the whole range. In 2-8 GHz, μ'' is positive.[41] Therefore, all the tested samples combine dielectric loss and magnetic loss. A gratifying result that μ'' of Ni/Ni$(OH)_2$ is larger than that of other reported values over the majority of the 2-18 GHz range. If the μ'' is positive, magnetic materials have energy loss. If the value is negative, there is no absorption. Though Ni is recognized in the study as an EM wave absorbing material owning excellent magnetic loss property, μ'' of four samples becomes negative at different frequency range (8.5 GHz for smooth chains and at 13 GHz for the other three samples).

As shown in Fig. 12, the RL of the four samples clearly demonstrates the morphology-dependence of the EM wave absorption performances: 1D structure (chain) has the lowest μ'', because of huge aspect ratio and the anisotropy of the material, while the 2D structure (ring) has the lowest ε'' .From the comparison among the reported superfine NPs and flowerlike nickel,[85,141] the smooth chain and rings demonstrate better performance. Compared with pure nickel nanomaterial, the advantage of Ni/Ni$(OH)_2$ hexagonal plates is that they have lots of interfaces, in which the lag of polarization between Ni and Ni $(OH)_2$ interfaces can occur. The impedances are matched well on the performance of the microwave absorption that is not negligible. It is noted that the urchin-like nickel chains show great potential as excellent absorbers as they exhibit the best RL value because of the high μ_i, point discharge effect, and multiple absorption. Note that the geometrical effect is an important reason for excellent properties.

Compared with the randomly dispersed NPs synthesized without external influence, magnetic nanostructures (such as cobalt) with

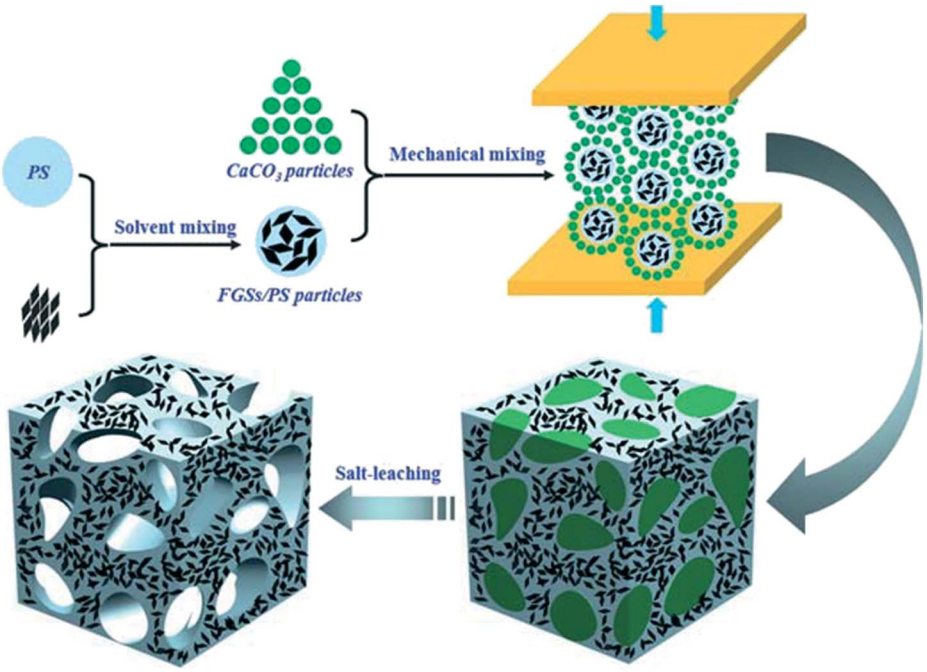

Fig. 5 Schematic diagram for preparation of porous PNCs consisting of functionalized graphene sheet (FGS) in polystyrene (PS).[97]Adapted with permissions from Royal Society of Chemistry.

aligned morphologies (well-defined rod or chain structures) via a γ-irradiation assisted route under a magnetic field (Fig. 13) are found to be able to increase the magnetization and coercivity of the material. This is attributed to the strong shape anisotropy of the composite materials (Fig. 14).[149]

The interaction of the cobalt NPs can affect the EM wave absorption property (Fig. 15).[149] When the applied magnetic field is about 1000 Gauss, the frequency range with RL > -4 dB occurs in the 10.4-15.6 GHz. In particular, a minimum RL value of -5.0 dB is observed at 13.8 GHz with a matching thickness of 2 mm. At 2000 G, the Cobalt nanostructures exhibit RL > -4 dB in the 9-16 GHz range, with a minimum RL value of -7 dB observed at 12.6 GHz. Further increasing the strength of magnetic field to 2500 Gauss, the best morphological of Co nanostructure is produced. When the magnetic field reaching the maximum of 3000 G, a minimum RL of -8.8 dB at 11.0 GHz is observed for the cobalt NPs.

This tendency might be caused by the geometrical effect of the Co nanostructures. In other words, the magnetic field-assisted synthesis method can produce magnetic NPs with specific morphology to enhance the electromagnetic wave absorption efficiencies by adjusting the magnetic field. The alignment effect is not achieved by simply using randomly dispersed particles.

In addition to Co nanostructures, Ni nanochains can also be synthesized by the γ-irradiation with the magnetic field-assisted process.[149] When a strength of 3000 G magnetic field was added, the diameters of about 100-200 nm Ni nanochains appeared. the surface of nanochain is smooth. Without any magnetic field assistance, only Ni NPs were formed by a direct γ-irradiation. On the other hand, the Ni nanochains can also be prepared using surfactant sodium dodecyl benzene sulfonate (SDBS) as structure-directing agent produced. The disadvantage of this method without magnetic field-assistance is the low-yield and the presence of a great number of individual Ni nanoparticles. These nanochains demonstrate a stinger-like morphology. The existence of magnetic field is one key factor of enhancing reproducible Ni nanochains with controlled morphologies.

The magnetic field can affect the preparation of Ni nanochains through the change of the RL value, shown in Fig. 16. The Ni nanochains with stinger-like surfaces and scattered Ni NPs show an RL value of -12 dB, and a bandwidth of 6.4-8.8 GHz. The smooth Ni nanochains show an absorption peak of -17.5 dB; meanwhile, the RL is above -4 dB in the frequency range of 6.0 - 10.6 GHz by a magnetic field-assisted method.

From the RL values of Ni nanowires[150] and MWNTs composites,[151] the geometrical effect is also a determining factor of EM wave absorption. The equation d = n/4 (n = 1, 3, 5, ...) states that when the thickness (d) matches λ_m, the reflected waves at the interface are totally canceled.[149] In conclusion, the specific morphology of the magnetic NPs is a determining factor of enhancing the geometrical effect that leads to the improved EM wave absorption.

3.3. Conductive polymer-based nanofillers

Intrinsically conducting polymers such as polyaniline, polypyrrole, and polyacetylene have been found to be promising materials for EMI shielding.[34,35] The EM radiation can be reduced or eliminated by conductive polymers because of their high σ, ε, and the ease of control of their σ and ε through different chemical processing such

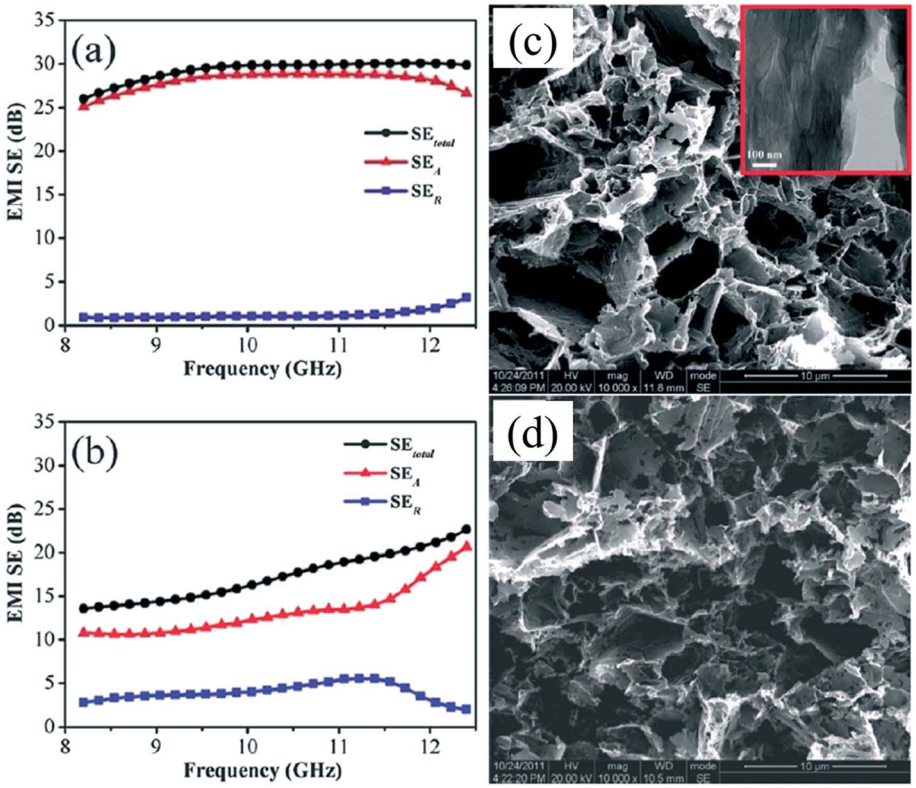

Fig. 6 EMI parameters in the X-band, and SEM images for (a, c) GPS045 and (b, d) GPS027. The inset in (c) shows the states of the embedded functionalized graphene sheets in the composites.[97]Adapted with permissions from Royal Society of Chemistry.

as molecular weight, doping level, counter ion, solvent, etc.[35] Again, the advantages of conductive polymers for EMI shielding include their relatively lightweight compared with metals, flexibility, and corrosion resistance.

Based on the theory of EMI shielding, the shielding effect is positively correlated with the σ of the material. As a good-conductor material (tanΔ >> 1), the SE of monolayer films can be calculated by the Eq. (19):

where $\Delta = \sqrt{\frac{2}{2\mu_0\omega\sigma}}$ is the skin depth. For an electrically thin shielding material, this is reduced to

where Z_0 = 376.7 V, which is the wave impedance of free space, 1/σd is about 10 Ω, the value of $20\log\left(\frac{1}{\sigma d}+\frac{Z_0}{2}\right)$ is determined by Z_0. Therefore, the SE is a linear function of log (σd).[14] The relationship of the measured electromagnetic interference SE with the σ_{dc} (dc conductivity) by the thickness is showed in Fig. 17. From Eq. (29), the positive correlation is established between the EMI SE and the σd, where σ and the thickness are the internal and external cause for the SE, respectively.

Although conductive polymers have demonstrated promising EMI shielding performance,[28,31,33] their prospects for broader

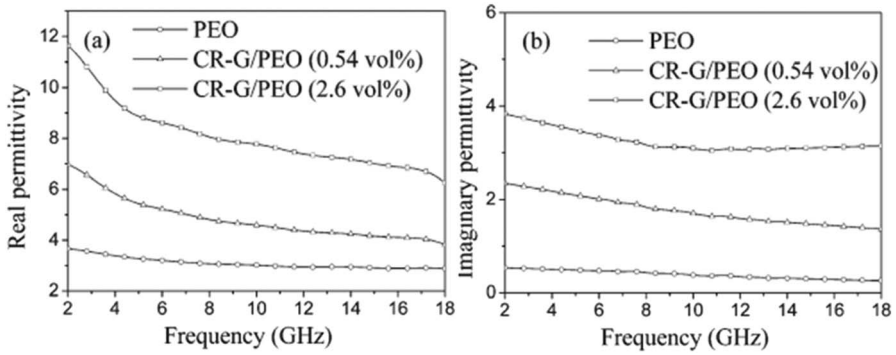

Fig. 7 The real permittivity (a) and imaginary permittivity (b) curves plotted against frequency for the composites.[80]Adapted with permissions from American Chemical Society.

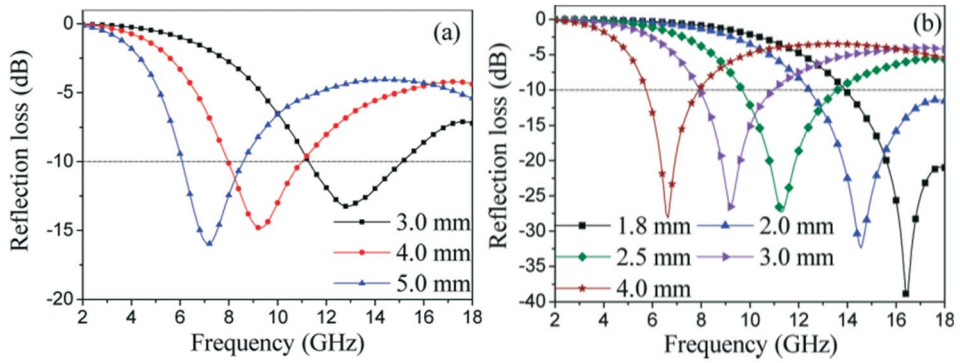

Fig. 8 Reflection loss spectra of (a) 0.54 and (b) 2.6 vol % loading of CR-G in PEO matrix at different thicknesses plotted against frequency.[80] Adapted with permissions from American Chemical Society.

applications are limited mainly due to their environmental stability and the fact that conductive polymers are not melt-processible in their conductive form.[34] Alternatively, melt-processible thermoplastic composite materials like polyvinyl chloride (PVC) or nylon still exhibit better conductivities than carbon black as fillers filled with polyaniline.[34]

3.4. Other carbon-based conductive nanofillers

Compared with solid powders, the powder of the porous structure owns larger dielectric loss. The porous carbons including carbon foams have been reported as an ideal candidate to develop effective EM wave absorbers.[152–154] In addition, composites consisted of porous carbon and a second functional component exhibit even better performance as potential light-weight EMI shielding materials over porous carbon-only materials.[154] For example, porous carbon/Co nanocomposites exhibit better EM wave absorption property than porous carbon alone by utilizing dielectric loss. Perhaps the porous carbon/Co nanocomposites present large quantities of interfaces to contribute to strong interfacial polarization.[155] The primary microwave absorptive mechanism is the dielectric loss. It has also been reported that unpurified SWNTs with small amounts of magnetic Fe NPs exhibit better microwave absorption properties, the effect of the synergy between the Fe and CNTs.[156] In addition, other composites consisting of CNTs and magnetic NPs such as $CoFe_2O_4$ can also absorb a large amount of EM wave due to the good matching between dielectric loss and magnetic loss.[157] Compared with Fe/CNTs and Fe@C composites,[158] carbon coated Ni nano-capsules[140] exhibit a relatively low ε"(~ 7.1-3.7), suggesting that improving the dispersion and reducing the magnetic coupling is a key factor in the graphite shells of the carbon coated Ni nano-capsules.[159] Meanwhile, graphite shells are efficient EM wave absorption materials, like CNTs through coating the outside of the magnetic cores and forming nano-capsules, they show the combined properties of the parent materials.[157,159] Therefore, the excellent EM wave absorbing properties of Ni@C are believed to be ascribed to the strong natural resonance and the delay phenomenon of polarization, in addition to the EM match in microstructure.[140] Promising EM wave absorptive materials could be developed from core-shell nano-architectures with dielectric shells and ferromagnetic cores.

$$SE_I = 10\log\left\{\frac{1}{4}\left[\frac{\sigma}{2\omega\epsilon_0}\left(\cosh\frac{2d}{\Delta}-\cos\frac{2d}{\Delta}\right)+\sqrt{\frac{\sigma}{2\omega\epsilon_0}}\left(\sinh\frac{2d}{\Delta}+\sin\frac{2d}{\Delta}\right)+2\left(\cosh\frac{2d}{\Delta}-\cos\frac{2d}{\Delta}\right)\right]\right\} \quad (28)$$

$$SE \approx 20\log\left(1+\frac{Z_0\sigma d}{2}\right) = 20\log(\sigma d)+20\log\left(\frac{1}{\sigma d}+\frac{Z_0}{2}\right) \quad (29)$$

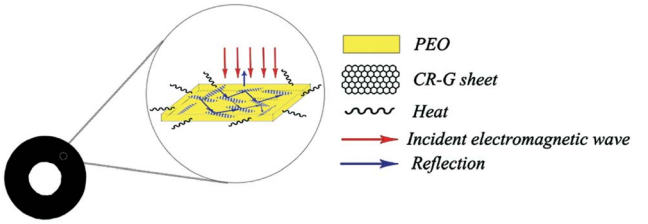

Fig. 9 Schematic diagram for the transport pathway of EM waves in the CR-G/PEO composites.[80]Adapted with permissions from American Chemical Society.

4. Conclusion and perspective

An up-to-date knowledge of the EMI shielding materials based on polymer nanocomposites reinforced with three types of conductive fillers has been reviewed. The frequency dependence of reflection loss, size- and morphology- controlled enhancement in EMI

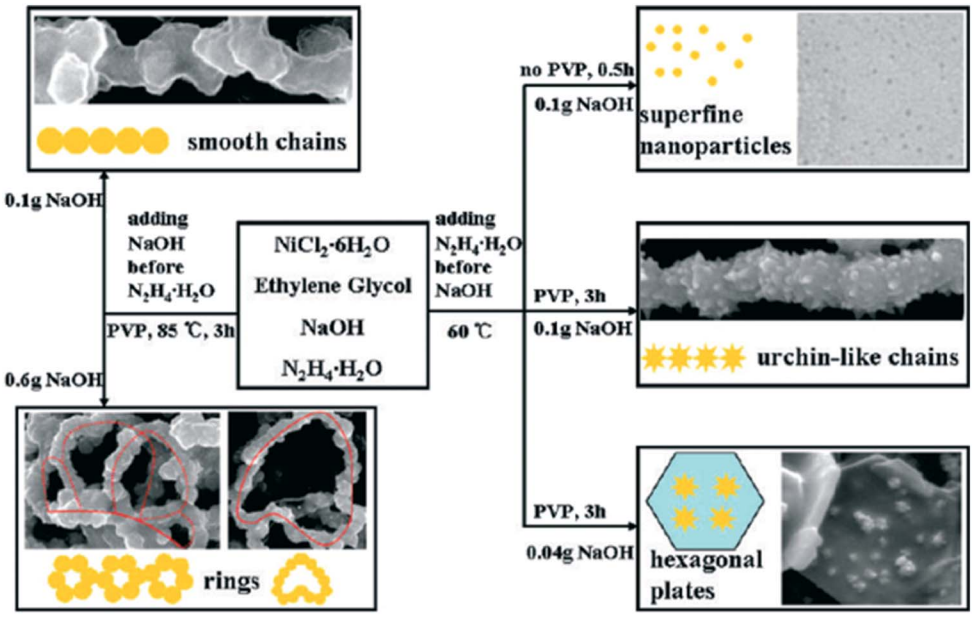

Fig. 10 Schematic illustration of nickel nanostructures with different morphologies.[41] Adapted with permissions from American Chemical Society.

shielding performance, and the mechanism of these different systems were critically discussed. Moreover, the effective complement between the dielectric loss and the magnetic loss can result in further enhanced EMI shielding effectiveness. From the various results obtained, the combination of different conductive fillers in one polymer nanocomposite system has demonstrated unique synergistic

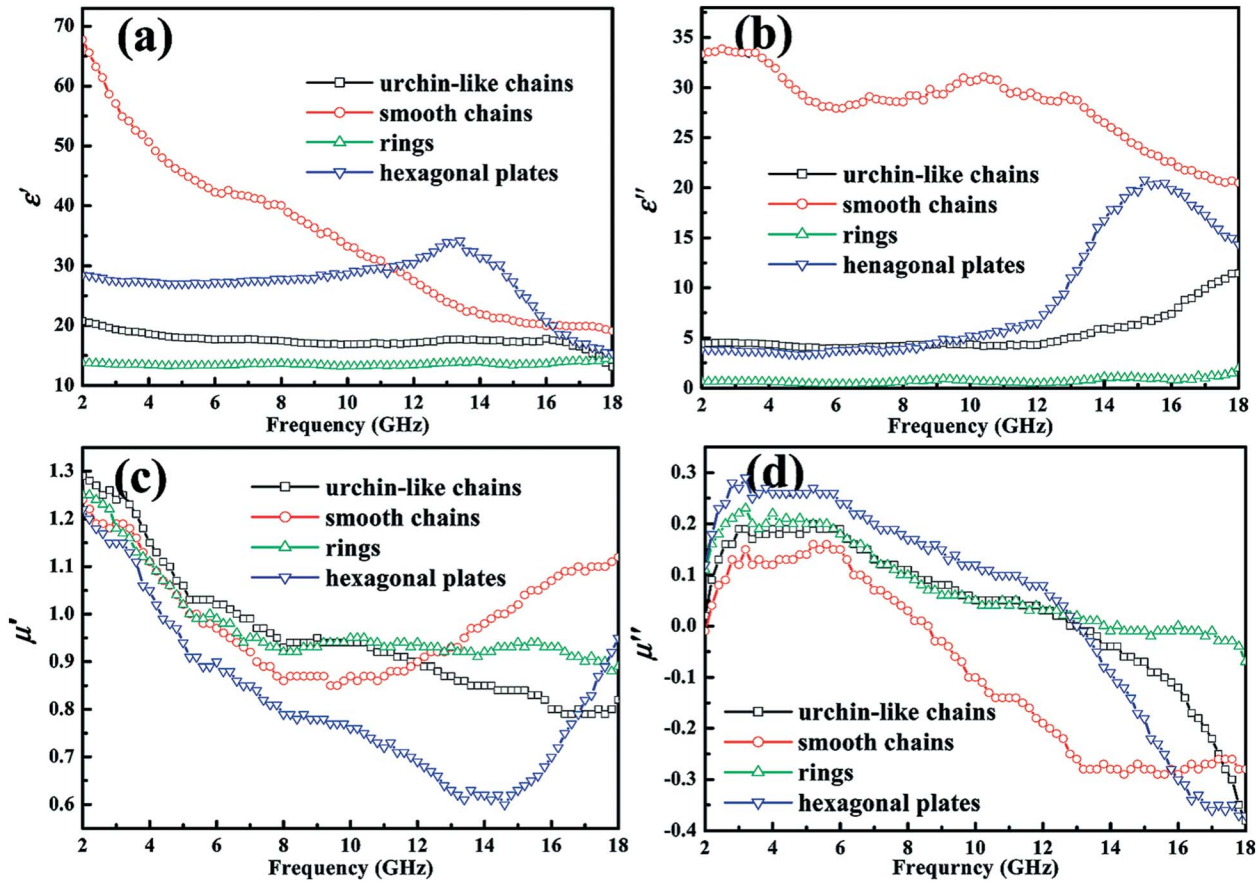

Fig. 11 EM parameters (a) ε_r' and (b) ε_r"; (c) μ_r' and (d) μ_r" curves plotted against frequency for the nickel samples with four different morphologies.[41] Adapted with permissions from American Chemical Society.

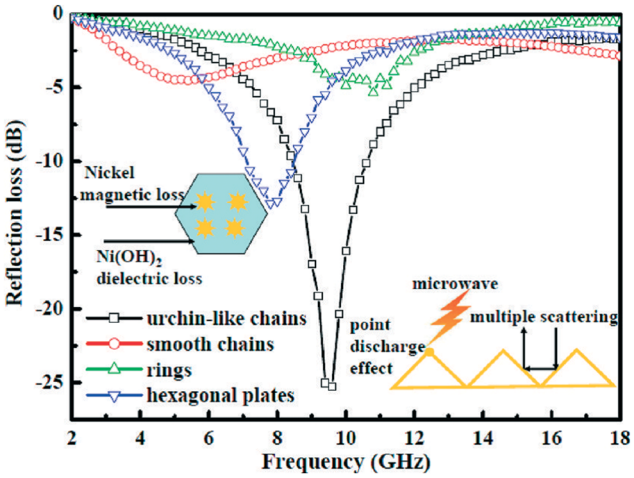

Fig. 12 Reflection loss of nickel samples (thicknesses of 2 mm) with four different morphologies. The left inset is the diagram of $Ni/Ni(OH)_2$ plates that combines magnetic and dielectric loss mechanisms. The right inset is the illustration scheme of how the urchin-like chain structure absorbs EM wave and enhances absorbing ability.[41] Adapted with permissions from American Chemical Society.

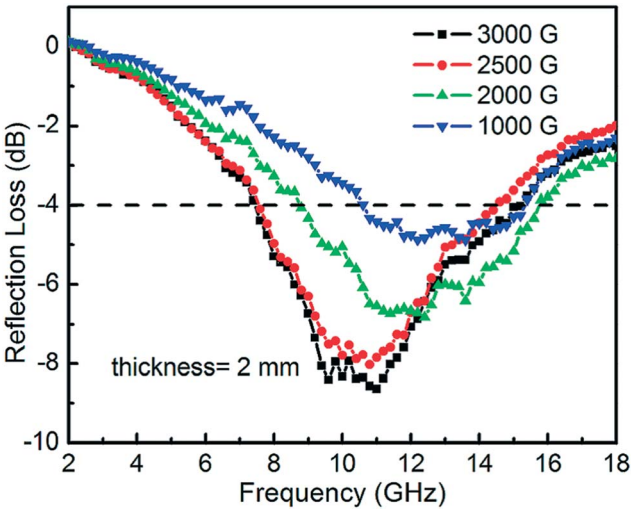

Fig. 15 EM wave absorption behaviors of the cobalt nanostructures prepared by γ-irradiation from 1000 G to 3000 G.[149] Adapted with permissions from American Chemical Society.

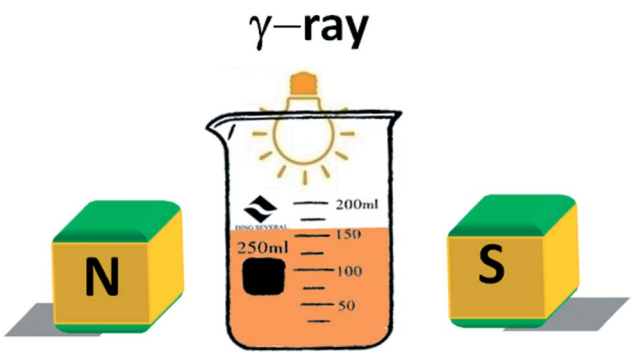

Fig. 13 Schematic experimental set up of the synthesis of nanochain-like magnetic nanostructures through a γ-Irradiation induced reduction route in the magnetic field.[149] Redrawn from ref.149

effects on the physicochemical properties of the resulting PNCs, which further play a significant role in enhancing the EMI shielding performance.

The excellent EMI shielding behaviors of unique morphology controlled nanostructures in the polymer nanocomposites suggest the potential applications in functional electromagnetic shield devices. However, the EMI SE is still limited due to ingredients with high density of metal component, eddy current loss, skin depth, and mismatch between the dielectric loss and the magnetic loss. Although the complicated mechanism has not been unearthed entirely, the uses of these combined conductive fillers with different compositions are helpful to solve the aforementioned problems. Hence, the well defined architectures of hierarchical nanostructures including the tunable filler configuration, size, density, specific surface area,

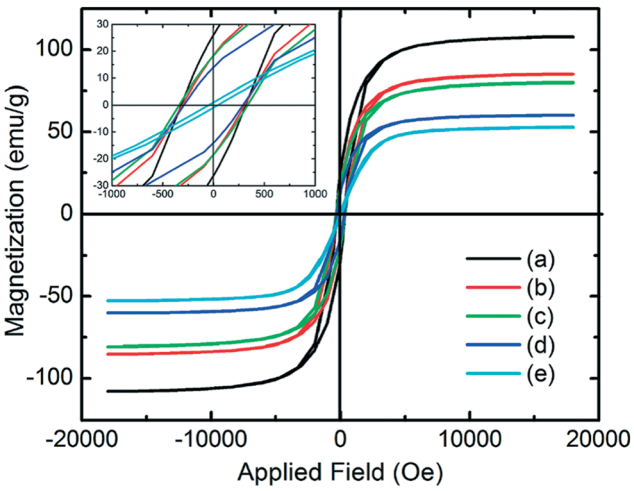

Fig. 14 Hysteresis loop of the the Co nanostructures with external magnetic fields of: (a) 3000, (b) 2500, (c) 2000, (d) 1000, and (e) 0 G. Insert shows the different coercive force with different external magnetic fields.[149] Adapted with permissions from American Chemical Society.

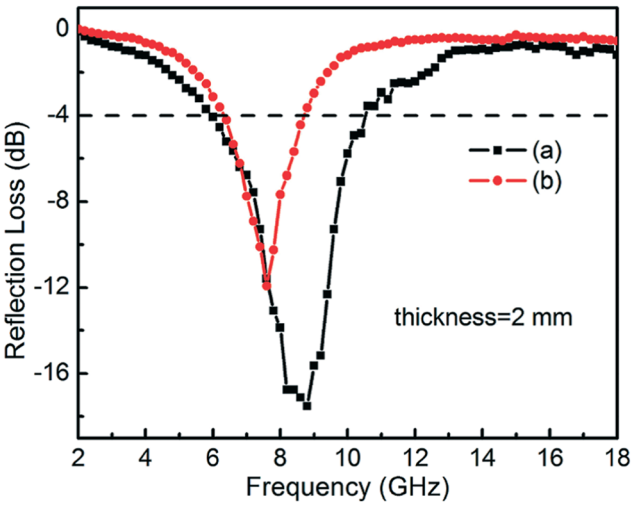

Fig. 16 EM wave absorption properties of the nickle nanostructures prepared by synthesis by (a) magnetic field-assisted and (b) surfactant-assisted without magnetic field-assisted.[149] Adapted with permissions from American Chemical Society.

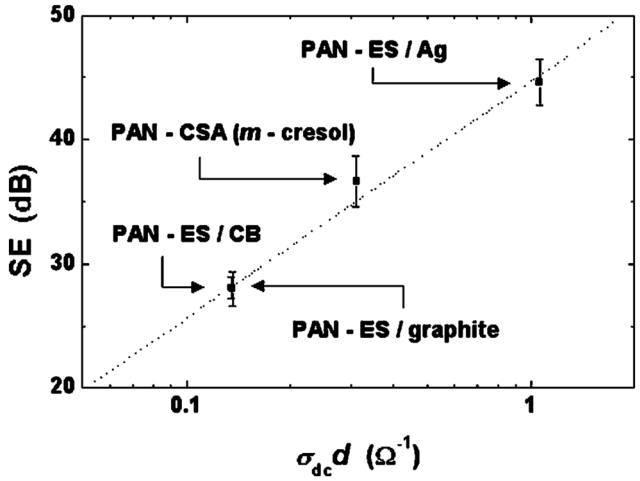

Fig. 17 Measured EMI SE as a function of the product of σ_{dc} by the sample thickness (d).[14]Adapted with permissions from American Institute of Physics.

composition are desirable for designing and fabricating light weight electrically conductive PNCs with controllable dielectric permittivity and magnetic permeability. Particularly, hierarchical nanostructures such as hollow CNTs and large surface area graphene decorated with different magnetic and dielectric nanostructures are envisioned to be excellent nanofillers for the next generation EMI shielding materials.

Conflict of interest

The authors declare that they have no conflict of interest.

Acknowledgement

The authors acknowledge the financial support from the National Natural Science Foundation of China (No. 51572157), the Fundamental Research Funds of Shandong University (2015JC016, 2015JC036), the Science and Technology Development Plan (2014GGX102004).

References

1 D. Chung, *Carbon*, 2001, **39**, 279–285.
2 S. Biswas, S. S. Panja and S. Bose, *J. Phys. Chem. C*, 2017, **121**, 13998–14009.
3 M. H. Al-Saleh and U. Sundararaj, *Carbon*, 2009, **47**, 1738–1746.
4 T. K. Gupta, B. P. Singh, R. B. Mathur and S. R. Dhakate, *Nanoscale*, 2014, **6**, 842–851.
5 S. Kwon, R. Ma, U. Kim, H. R. Choi and S. Baik, *Carbon*, 2014, **68**, 118–124.
6 W. L. Song, M. S. Cao, M. M. Lu, S. Bi, C. Y. Wang, J. Liu, J. Yuan and L. Z. Fan, *Carbon*, 2014, **66**, 67–76.
7 B. Wei, R. Spolenak, P. Kohler-Redlich, M. Rühle and E. Arzt, *Appl. Phys. Lett.*, 1999, **74**, 3149–3151.
8 M. H. Al-Saleh, W. H. Saadeh and U. Sundararaj, *Carbon*, 2013, **60**, 146–156.
9 Z. Chen, C. Xu, C. Ma, W. Ren and H. M. Cheng, *Adv. Mater.*, 2013, **25**, 1296–1300.
10 D. Ding, Y. Shi, Z. Wu, W. Zhou, F. Luo and J. Chen, *Carbon*, 2013, **60**, 552–555.
11 M. Mahmoodi, M. Arjmand, U. Sundararaj and S. Park, *Carbon*, 2012, **50**, 1455–1464.
12 P. Saini, V. Choudhary, N. Vijayan and R. Kotnala, *J. Phys. Chem. C*, 2012, **116**, 13403–13412.
13 B. Wang, Q. Cao and S. Zhang, *Mater. Sci. Semicond. Process.*, 2014, **19**, 101–106.
14 J. Joo and C. Lee, *J. Appl. Phys.*, 2000, **88**, 513–518.
15 Z. Guo, S. Park, H. T. Hahn, S. Wei, M. Moldovan, A. B. Karki and D. P. Young, *J. Appl. Phys.*, 2007, **101**, 09M511.
16 J.-M. Thomassin, C. Pagnoulle, L. Bednarz, I. Huynen, R. Jerome and C. Detrembleur, *J. Mater. Chem.*, 2008, **18**, 792–796.
17 Y. Yang, M. C. Gupta, K. L. Dudley and R. W. Lawrence, *Nano Lett.*, 2005, **5**, 2131–2134.
18 H. Kim, K. Kim, C. Lee, J. Joo, S. Cho, H. Yoon, D. Pejaković, J. Yoo and A. Epstein, *Appl. Phys. Lett.*, 2004, **84**, 589–591.
19 S. E. Lee, O. Choi and H. T. Hahn, *J. Appl. Phys.*, 2008, **104**, 033705.
20 G. S. Chaubey, C. Barcena, N. Poudyal, C. Rong, J. Gao, S. Sun and J. P. Liu, *J. Am. Chem. Soc.*, 2007, **129**, 7214–7215.
21 G. Sun, B. Dong, M. Cao, B. Wei and C. Hu, *Chem. Mater.*, 2011, **23**, 1587–1593.
22 P. Singh, V. Babbar, A. Razdan, S. Srivastava and T. Goel, *Mater. Sci. Eng. B-Adv.*, 2000, **78**, 70–74.
23 Z. Haijun, L. Zhichao, M. Chengliang, Y. Xi, Z. Liangying and W. Mingzhong, *Mater. Sci. Eng. B-Adv.*, 2002, **96**, 289–295.
24 X. C. Sun and N. Nava, *Nano Lett.*, 2002, **2**, 765–769.
25 N. E. Kazantseva, J. Vilčáková, V. Křesálek, P. Sáha, I. Sapurina and J. Stejskal, *J. Magn. Magn. Mater.*, 2004, **269**, 30–37.
26 P. Xu, X. Han, J. Jiang, X. Wang, X. Li and A. Wen, *J. Phys. Chem. C*, 2007, **111**, 12603–12608.
27 X. Dong, X. Zhang, H. Huang and F. Zuo, *Appl. Phys. Lett.*, 2008, **92**, 013127–013127.
28 W. Wang, S. P. Gumfekar, Q. Jiao and B. Zhao, *J. Mater. Chem. C*, 2013, **1**, 2851–2859.
29 C. Basavaraja, E. Jo, B. S. Kim, D. G. Kim and D. S. Huh, *Polym. Eng. Sci.*, 2011, **51**, 54–61.
30 J. Azadmanjiri, P. Hojati-Talemi, G. Simon, K. Suzuki and C. Selomulya, *Polym. Eng. Sci.*, 2011, **51**, 247–253.
31 A. Ohlan, K. Singh, A. Chandra and S. Dhawan, *Appl. Phys. Lett.*, 2008, **93**, 053114–053114.
32 T. Kasagi, S. Suenaga, T. Tsutaoka and K. Hatakeyama, *J. Magn. Magn. Mater.*, 2007, **310**, 2566–2568.
33 D. A. Makeiff and T. Huber, *Synth. Met.*, 2006, **156**, 497–505.
34 N. F. Colaneri and L. Schacklette, *IEEE T. Instrum. Meas.*, 1992, **41**, 291–297.
35 J. Joo and A. Epstein, *Appl. Phys. Lett.*, 1994, **65**, 2278–2280.
36 Z. Liu, G. Bai, Y. Huang, Y. Ma, F. Du, F. Li, T. Guo and Y. Chen, *Carbon*, 2007, **45**, 821–827.
37 R. B. Schulz, V. C. Plantz and D. R. Brush, *IEEE T. Electromagn. C.*, 1988, **30**, 187–201.
38 M. Chen, L. Zhang, S. Duan, S. Jing, H. Jiang, M. Luo and C. Li, *Nanoscale*, 2014, **6**, 3796–3803.
39 J. Zhu, S. Wei, N. Haldolaarachchige, D. P. Young and Z. Guo, *J. Phys. Chem. C*, 2011, **115**, 15304–15310.
40 R. Lv, A. Cao, F. Kang, W. Wang, J. Wei, J. Gu, K. Wang and D. Wu, *J. Phys. Chem. C*, 2007, **111**, 11475–11479.
41 C. Wang, X. Han, P. Xu, J. Wang, Y. Du, X. Wang, W. Qin and T. Zhang, *J. Phys. Chem. C*, 2010, **114**, 3196–3203.
42 H. Meng, Z. H. Wang and C. X. Hu, *Mater. Prot.*, 2006, **39**, 17–19.
43 J. Huo, L. Wang and H. Yu, *J. Mater. Sci.*, 2009, **44**, 3917–3927.
44 J. R. Liu, M. Itoh and K.-i. Machida, *Appl. Phys. Lett.*, 2006, **88**, 062503.
45 W. A. Roshen, C. S. Korman and W. Daum, *J. Appl. Phys.*, 2005, **97**, 10Q701.
46 T. Renbarger, J. L. Dotson and G. Novak, *Appl. Opt.*, 1998, **37**, 6643–6647.
47 W. H. Jeong, Y. H. Han and B. M. Song, *J. Appl. Phys.*, 2002, **91**, 7619–7621.
48 K. Sun, Z. Lan, Z. Yu, Z. Xu, X. Jiang, Z. Wang, Z. Liu and M. Luo, *J. Appl. Phys.*, 2011, **109**, 106103.
49 M. Meshram, N. K. Agrawal, B. Sinha and P. Misra, *J. Magn. Magn. Mater.*, 2004, **271**, 207–214.
50 J. Zhu, Q. He, Z. Luo, A. Khasanov, Y. Li, L. Sun, Q. Wang, S. Wei and Z. Guo, *J. Mater. Chem.*, 2012, **22**, 15928–15938.
51 X. Zhang, O. Alloul, J. Zhu, Q. He, Z. Luo, H. A. Colorado, N. Haldolaarachchige, D. P. Young, T. Shen and S. Wei, *RSC Adv.*, 2013, **3**, 9453–9464.
52 X. Zhang, Q. He, H. Gu, H. A. Colorado, S. Wei and Z. Guo, *ACS Appl. Mater. Interfaces*, 2013, **5**, 898–910.
53 Q. He, T. Yuan, S. Wei, N. Haldolaarachchige, Z. Luo, D. P. Young, A. Khasanov and Z. Guo, *Angew. Chem.*, 2012, **124**, 8972–8975.

54 Q. He, T. Yuan, J. Zhu, Z. Luo, N. Haldolaarachchige, L. Sun, A. Khasanov, Y. Li, D. P. Young and S. Wei, *Polymer*, 2012, **53**, 3642–3652.
55 Q. He, T. Yuan, Z. Luo, N. Haldolaarachchige, D. P. Young, S. Wei and Z. Guo, *Chem. Commun.*, 2013, **49**, 2679–2681.
56 Q. He, T. Yuan, X. Zhang, Z. Luo, N. Haldolaarachchige, L. Sun, D. P. Young, S. Wei and Z. Guo, *Macromolecules*, 2013, **46**, 2357–2368.
57 Q. He, T. Yuan, X. Yan, Z. Luo, N. Haldolaarachchige, D. P. Young, S. Wei and Z. Guo, *Chem. Commun.*, 2014, **50**, 201–203.
58 Q. He, T. Yuan, S. Wei and Z. Guo, *JOM*, 2014, **66**, 655–659.
59 J. Zhu, S. Wei, M. Alexander Jr, T. D. Dang, T. C. Ho and Z. Guo, *Adv. Funct. Mater.*, 2010, **20**, 3076–3084.
60 C. Jianrong, M. Yuqing, H. Nongyue, W. Xiaohua and L. Sijiao, *Biotechnol. Adv.*, 2004, **22**, 505–518.
61 W. Chen, L. Feng and B. Qu, *Chem. Mater.*, 2004, **16**, 368–370.
62 H. Zou, S. Wu and J. Shen, *Chem. Rev.*, 2008, **108**, 3893–3957.
63 E. K. Wujcik, N. J. Blasdel, D. Trowbridge and C. N. Monty, *IEEE Sens. J.*, 2013, **13**, 3430–3436.
64 E. K. Wujcik and C. N. Monty, *Wires. Nanomed. Nanobi.*, 2013, **5**, 233–249.
65 E. Dubois, J. Chevalet and R. Massart, *J. Mol. Liq.*, 1999, **83**, 243–254.
66 R. Ma, Z. Liu, L. Li, N. Iyi and T. Sasaki, *J. Mater. Chem.*, 2006, **16**, 3809–3813.
67 J. Deng, X. Ding, W. Zhang, Y. Peng, J. Wang, X. Long, P. Li and A. S. Chan, *Polymer*, 2002, **43**, 2179–2184.
68 J.-M. Thomassin, X. Lou, C. Pagnoulle, A. Saib, L. Bednarz, I. Huynen, R. Jérôme and C. Detrembleur, *J. Phys. Chem. C*, 2007, **111**, 11186–11192.
69 N. Li, Y. Huang, F. Du, X. He, X. Lin, H. Gao, Y. Ma, F. Li, Y. Chen and P. C. Eklund, *Nano Lett.*, 2006, **6**, 1141–1145.
70 L. L. Wang, B. K. Tay, K.-Y. See, Z. Sun, L.-K. Tan and D. Lua, *Carbon*, 2009, **47**, 1905–1910.
71 M. F. De Volder, S. H. Tawfick, R. H. Baughman and A. J. Hart, *Science*, 2013, **339**, 535–539.
72 M. Zhang, S. Fang, A. A. Zakhidov, S. B. Lee, A. E. Aliev, C. D. Williams, K. R. Atkinson and R. H. Baughman, *Science*, 2005, **309**, 1215–1219.
73 M. Zhang, K. R. Atkinson and R. H. Baughman, *Science*, 2004, **306**, 1358–1361.
74 U. Basuli, S. Chattopadhyay, C. Nah and T. K. Chaki, *Polym. Compos.*, 2012, **33**, 897–903.
75 W. L. Song, M. S. Cao, Z. L. Hou, J. Yuan and X.-y. Fang, *Scr. Mater.*, 2009, **61**, 201–204.
76 H. L. Zhu, Y. J. Bai, R. Liu, N. Lun, Y. X. Qi, F. D. Han and J. Q. Bi, *J. Mater. Chem.*, 2011, **21**, 13581–13587.
77 Z. Liu, G. Bai, Y. Huang, F. Li, Y. Ma, T. Guo, X. He, X. Lin, H. Gao and Y. Chen, *J. Phys. Chem. C*, 2007, **111**, 13696–13700.
78 G. Li, T. Xie, S. Yang, J. Jin and J. Jiang, *J. Phys. Chem. C*, 2012, **116**, 9196–9201.
79 J. Ling, W. Zhai, W. Feng, B. Shen, J. Zhang and W. g. Zheng, *ACS Appl. Mater. Interfaces*, 2013, **5**, 2677–2684.
80 X. Bai, Y. Zhai and Y. Zhang, *J. Phys. Chem. C*, 2011, **115**, 11673–11677.
81 H.-B. Zhang, Q. Yan, W. G. Zheng, Z. He and Z.-Z. Yu, *ACS Appl. Mater. Interfaces*, 2011, **3**, 918–924.
82 X. Zhang, Q. He, H. Gu, S. Wei and Z. Guo, *J. Mater. Chem.*, 2013, **100**, 2886–2899.
83 P. Saini, M. Arora, G. Gupta, B. K. Gupta, V. N. Singh and V. Choudhary, *Nanoscale*, 2013, **5**, 4330–4336.
84 H. Ding, X. M. Liu, M. Wan and S.-Y. Fu, *J. Phys. Chem. B*, 2008, **112**, 9289–9294.
85 P. Xu, X. Han, C. Wang, D. Zhou, Z. Lv, A. Wen, X. Wang and B. Zhang, *J. Phys. Chem. B*, 2008, **112**, 10443–10448.
86 S. C. Wuang, K. G. Neoh, E. T. Kang, D. W. Pack and D. E. Leckband, *J. Mater. Chem.*, 2007, **17**, 3354–3362.
87 J. Zhu, S. Wei, L. Zhang, Y. Mao, J. Ryu, P. Mavinakuli, A. B. Karki, D. P. Young and Z. Guo, *J. Phys. Chem. C*, 2010, **114**, 16335–16342.
88 P. Xu, X. Han, C. Wang, H. Zhao, J. Wang, X. Wang and B. Zhang, *J. Phys. Chem. B*, 2008, **112**, 2775–2781.
89 J. Zhou, J. He, G. Li, T. Wang, D. Sun, X. Ding, J. Zhao and S. Wu, *J. Phys. Chem. C*, 2010, **114**, 7611–7617.
90 P. Y. Keng, B. Y. Kim, I.-B. Shim, R. Sahoo, P. E. Veneman, N. R. Armstrong, H. Yoo, J. E. Pemberton, M. M. Bull and J. J. Griebel, *ACS Nano*, 2009, **3**, 3143–3157.
91 W. Li, T. Qiu, L. Wang, S. Ren, J. Zhang, L. He and X. Li, *ACS Appl. Mater. Interfaces*, 2013, **5**, 883–891.
92 X. Chen, S. Wei, C. Gunesoglu, J. Zhu, C. S. Southworth, L. Sun, A. B. Karki, D. P. Young and Z. Guo, *Macromol. Chem. Phys.*, 2010, **211**, 1775–1783.
93 M. S. Cao, J. Yang, W. L. Song, D. Q. Zhang, B. Wen, H. B. Jin, Z. L. Hou and J. Yuan, *ACS Appl. Mater. Interfaces*, 2012, **4**, 6949–6956.
94 K. Singh, A. Ohlan, V. H. Pham, R. Balasubramaniyan, S. Varshney, J. Jang, S. H. Hur, W. M. Choi, M. Kumar and S. Dhawan, *Nanoscale*, 2013, **5**, 2411–2420.
95 A. N. Aleshin, *Adv. Mater.*, 2006, **18**, 17–27.
96 H. Fischer, *Mater. Sci. Eng. C*, 2003, **23**, 763–772.
97 D. X. Yan, P. G. Ren, H. Pang, Q. Fu, M. B. Yang and Z. M. Li, *J. Mater. Chem.*, 2012, **22**, 18772–18774.
98 A. H. A. Hoseini, M. Arjmand, U. Sundararaj and M. Trifkovic, *Mater. Design*, 2017, **125**, 126–134.
99 C. Wen-Yen and C. Yung-Shin, *J. Appl. Polym. Sci.*, 1992, **46**, 673–681.
100 P. Saini, V. Choudhary, B. P. Singh, R. B. Mathur and S. K. Dhawan, *Mater. Chem. Phys.*, 2009, **113**, 919–926.
101 M. S. Kim, H. K. Kim, S. W. Byun, S. H. Jeong, Y. K. Hong, J. S. Joo, K. T. Song, J. K. Kim, C. J. Lee and J. Y. Lee, *Synth. Met.*, 2002, **126**, 233–239.
102 J. Liang, Y. Wang, Y. Huang, Y. Ma, Z. Liu, J. Cai, C. Zhang, H. Gao and Y. Chen, *Carbon*, 2009, **47**, 922–925.
103 V. Eswaraiah, V. Sankaranarayanan and S. Ramaprabhu, *Macromol. Mater. Eng.*, 2011, **296**, 894–898.
104 H. D. Huang, C. Y. Liu, D. Zhou, X. Jiang, G. J. Zhong, D.-X. Yan and Z. M. Li, *J. Mater. Chem. A.*, 2015, **3**, 4983–4991.
105 X.-B. Xu, Z.-M. Li, K. Dai and M.-B. Yang, *Appl. Phys. Lett.*, 2006, **89**, 032105.
106 Q. Liu, J. Gu, W. Zhang, Y. Miyamoto, Z. Chen and D. Zhang, *J. Mater. Chem.*, 2012, **22**, 21183–21188.
107 Y. Huang, Z. Xu, J. Shen, T. Tang and R. Huang, *Appl. Phys. Lett.*, 2007, **90**, 133117.
108 A. Al-Ghamdi, O. A. Al-Hartomy, F. Al-Solamy, A. A. Al-Ghamdi and F. El-Tantawy, *J. Appl. Polym. Sci.*, 2013, **127**, 2227–2234.
109 B. Lee, W. Woo, H. Park, H. Hahm, J. Wu and M. Kim, *J. Mater. Sci.*, 2002, **37**, 1839–1843.
110 B. S. Villacorta, A. A. Ogale and T. H. Hubing, *Polym. Eng. Sci.*, 2013, **53**, 417–423.
111 A. Das, C. M. Megaridis, L. Liu, T. Wang and A. Biswas, *Appl. Phys. Lett.*, 2011, **98**, 174101.
112 S. Chopra, M. K. Pandey and S. Alam, *J. Appl. Polym. Sci.*, 2011, **120**, 3204–3211.
113 M. H. Al-Saleh and U. Sundararaj, *J. Polym. Sci. Pol. Phys.*, 2012, **50**, 1356–1362.
114 Y. C. Chen, C. C. Li, Y. F. Lee, W. Chin, Y. H. Lin, S. Y. Lu, C. T. Hsu, S. H. Syue, H. J. Chen and B. Y. Wei, *J. Mater. Chem.*, 2008, **18**, 4616–4618.
115 M. Seo, J. Yim, Y. Ahn, F. Rotermund, D. Kim, S. Lee and H. Lim, *Appl. Phys. Lett.*, 2008, **93**, 231905.
116 C. C. M. Ma, Y. L. Huang, H. C. Kuan and Y. S. Chiu, *J. Polym. Sci. Pol. Phys.*, 2005, **43**, 345–358.
117 Y. Huang, N. Li, Y. Ma, F. Du, F. Li, X. He, X. Lin, H. Gao and Y. Chen, *Carbon*, 2007, **45**, 1614–1621.
118 D. Eder, *Chem. Rev.*, 2010, **110**, 1348–1385.
119 Y. P. Sun, K. Fu, Y. Lin and W. Huang, *Acc. Chem. Res.*, 2002, **35**, 1096–1104.
120 Q. He, T. Yuan, X. Yan, D. Ding, Q. Wang, Z. Luo, T. D. Shen, S. Wei, D. Cao and Z. Guo, *Macromol. Chem. Phys.*, 2014, **215**, 327–340.
121 H. Gu, J. Guo, Q. He, Y. Jiang, Y. Huang, N. Haldolaarachige, Z. Luo, D. P. Young, S. Wei and Z. Guo, *Nanoscale*, 2014, **6**, 181–189.
122 K. S. Novoselov, V. Fal, L. Colombo, P. Gellert, M. Schwab and K. Kim, *Nature*, 2012, **490**, 192–200.
123 A. Pénicaud and C. Drummond, *Acc. Chem. Res.*, 2012, **46**, 129–137.
124 C. Rao, H. R. Matte and K. Subrahmanyam, *Acc. Chem. Res.*, 2012, **46**, 149–159.
125 V. Georgakilas, M. Otyepka, A. B. Bourlinos, V. Chandra, N. Kim, K. C. Kemp, P. Hobza, R. Zboril and K. S. Kim, *Chem. Rev.*, 2012, **112**, 6156–6214.
126 J. Zhu, M. Chen, Q. He, L. Shao, S. Wei and Z. Guo, *RSC Adv.*, 2013, **3**, 22790–22824.
127 X. Zhang, O. Alloul, Q. He, J. Zhu, M. J. Verde, Y. Li, S. Wei and Z. Guo, *Polymer*, 2013, **54**, 3594–3604.
128 T. Kuilla, S. Bhadra, D. Yao, N. H. Kim, S. Bose and J. H. Lee, *Prog. Polym. Sci.*, 2010, **35**, 1350–1375.
129 Y. Chen, Y. Li, M. Yip and N. Tai, *Compos. Sci. Technol.*, 2013, **80**, 80–86.
130 C. Lei, D. Chen, B. Wu, Y. Xu, S. Li and W. Huang, *J. Appl. Polym. Sci.*, 2011, **121**, 3724–3732.

131 S. E. Zakiyan, H. Azizi and I. Ghasemi, *Compos. Sci. Technol.*, 2018, **157**, 217–227.

132 P. Tartaj, M. del Puerto Morales, S. Veintemillas-Verdaguer, T. González-Carreno and C. J. Serna, *J. Phys. D: Appl. Phys.*, 2003, **36**, R182.

133 D. L. Leslie-Pelecky and R. D. Rieke, *Chem. Mater.*, 1996, **8**, 1770–1783.

134 R. M. Crooks, M. Zhao, L. Sun, V. Chechik and L. K. Yeung, *Acc. Chem. Res.*, 2001, **34**, 181–190.

135 C. J. Murphy, T. K. Sau, A. M. Gole, C. J. Orendorff, J. Gao, L. Gou, S. E. Hunyadi and T. Li, *J. Phys. Chem. B*, 2005, **109**, 13857–13870.

136 G. G. Bush, *J. Appl. Phys.*, 1988, **63**, 3765–3767.

137 T. Nakamura, *J. Appl. Phys.*, 2000, **88**, 348–353.

138 J. Zhang, S. Xu and E. Kumacheva, *J. Am. Chem. Soc.*, 2004, **126**, 7908–7914.

139 H. McConnell, *IEEE Trans. Commun.*, 1954, **73**, 226–235.

140 X. Zhang, X. Dong, H. Huang, Y. Liu, W. Wang, X. Zhu, B. Lv, J. Lei and C. Lee, *Appl. Phys. Lett.*, 2006, **89**, 053115.

141 C.-C. Lee and D.-H. Chen, *Appl. Phys. Lett.*, 2007, **90**, 193102–193103.

142 S.-S. Kim, S.-T. Kim, Y.-C. Yoon and K.-S. Lee, *J. Appl. Phys.*, 2005, **97**, 10F905.

143 C. Wang, X. Han, X. Zhang, S. Hu, T. Zhang, J. Wang, Y. Du, X. Wang and P. Xu, *J. Phys. Chem. C*, 2010, **114**, 14826–14830.

144 S.-S. Kim, S.-T. Kim, J.-M. Ahn and K.-H. Kim, *J. Magn. Magn. Mater.*, 2004, **271**, 39–45.

145 H. T. Zhao, X. J. Han, L. F. Zhang, G. Y. Wang, C. Wang, X. A. Li and P. Xu, *Radiat. Phys. Chem.*, 2011, **80**, 390–393.

146 Y. Deng, X. Liu, B. Shen, L. Liu and W. Hu, *J. Magn. Magn. Mater.*, 2006, **303**, 181–184.

147 Y. Wang and J. J. Ke, *Mater. Res. Bull.*, 1996, **31**, 55–61.

148 H. Zhao, X. Sun, C. Mao and J. Du, *Physica B (Amsterdam, Neth.)*, 2009, **404**, 69–72.

149 H. Zhao, B. Zhang, J. Zhang, L. Zhang, X. Han, P. Xu and Y. Zhou, *J. Phys. Chem. C*, 2010, **114**, 21214–21218.

150 B. Gao, L. Qiao, J. Wang, Q. Liu, F. Li, J. Feng and D. Xue, *J. Phys. D: Appl. Phys.*, 2008, **41**, 235005.

151 L. Deng and M. Han, *Appl. Phys. Lett.*, 2007, **91**, 023119.

152 J. Yang, Z. M. Shen and Z. B. Hao, *Carbon*, 2004, **42**, 1882–1885.

153 Z. Fang, C. Li, J. Sun, H. Zhang and J. Zhang, *Carbon*, 2007, **45**, 2873–2879.

154 Q. Liu, D. Zhang, T. Fan, J. Gu, Y. Miyamoto and Z. Chen, *Carbon*, 2008, **46**, 461–465.

155 Q. Liu, D. Zhang and T. Fan, *Appl. Phys. Lett.*, 2008, **93**, 013110.

156 A. Wadhawan, D. Garrett and J. Perez, *Appl. Phys. Lett.*, 2003, **83**, 2683–2685.

157 R. Che, C. Zhi, C. Liang and X. Zhou, *Appl. Phys. Lett.*, 2006, **88**, 033105.

158 R. Che, L. M. Peng, X. F. Duan, Q. Chen and X. Liang, *Adv. Mater.*, 2004, **16**, 401–405.

159 J. R. Liu, M. Itoh, T. Horikawa, K.-i. Machida, S. Sugimoto and T. Maeda, *J. Appl. Phys.*, 2005, **98**, 054305–054307.

